1957

Range-energy relation for liquid hydrogen bubble chambers

Clark, Glenwood, Jr

Monterey, California: Naval Postgraduate School, 1957.

http://hdl.handle.net/10945/14546

RANGE-ENERGY RELATION FOR LIQUID HYDROGEN BUBBLE CHAMBERS

Glenwood Clark, Jr.
and
William F. Diehl

RANGE-ENERGY RELATION FOR LIQUID HYDROGEN BUBBLE CHAMBERS

by

Glenwood Clark, Jr., and William F. Diehl

Lieutenants, United States Navy

Submitted in partial fulfillment of
the requirements for the degree of

MASTER OF SCIENCE
IN
PHYSICS

United States Naval Postraduate School
Monterey, California

1957

RANGE-ENERGY RELATION FOR LIQUID HYDROGEN BUBBLE CHAMBERS

* * * * *

Glenwood Clark, Jr.,

William F. Diehl

RANGE-ENERGY RELATION
FOR LIQUID HYDROGEN BUBBLE CHAMBERS

by

Glenwood Clark, Jr.
William F. Diehl

This work is accepted as fulfilling

the thesis requirements for the degree of

MASTER OF SCIENCE

IN

PHYSICS

from the

United States Naval Postgraduate School

UCRL-3789

UNIVERSITY OF CALIFORNIA
Radiation Laboratory
Berkeley, California

Contract No. W-7405-eng-48

RANGE-ENERGY RELATION FOR LIQUID HYDROGEN BUBBLE CHAMBERS

Glenwood Clark, Jr., and William F. Diehl

(M.S. Thesis)

May 1957

Submitted in partial fulfillment of
the requirements for the degree of
MASTER OF SCIENCE
in
PHYSICS

United States Naval Postgraduate School
Monterey, California

Printed for the U.S. Atomic Energy Commission

RANGE-ENERGY RELATION FOR LIQUID HYDROGEN BUBBLE CHAMBERS

Glenwood Clark, Jr., and William F. Diehl

Radiation Laboratory
University of California
Berkeley, California

May 1957

ABSTRACT

In studying the kinematics of the formation, reactions, and decay of unstable strange particles such as $K^{\pm}$, Λ^0, θ^0, and $\Sigma^{\pm}$ with a liquid hydrogen bubble chamber a range-energy relation is essential. To obtain such a relation, one must know the density of superheated liquid parahydrogen. Heretofore, this density has not been determined. Direct measurement by conventional means of the density of the liquid hydrogen in the bubble chamber is difficult because the liquid is superheated for only 20 to 30 milliseconds.

To determine the density, the mean range of μ^+ mesons produced by π^+ mesons decaying at rest in the 10-inch UCRL liquid hydrogen bubble chamber was measured and found to be 1.103 ± 0.003 cm (standard deviation 5.0%; 444 $\pi \rightarrow \mu \rightarrow e$ events). From the Bethe-Bloch theory and a μ^+ kinetic energy of 4.12 ± 0.02 Mev., this value of range gave a density of $(5.83 \pm .06) \times 10^{-2}$ g/cm^3 for superheated liquid parahydrogen. The temperature and pressure of the hydrogen during the sensitive time were 27.6 ± 0.1°K and 48 ± 5 psia. A plot of the range-energy relation for protons, π, μ, K, Σ, and Ξ particles based on Bethe-Bloch theory, and the above value of density is given for kinetic energy values ranging from 1 to 1000 Mev.

- - - - - - - - - - - - - - -

We wish to express our appreciation to Dr. Luis W. Alvarez, head of the Hydrogen Bubble Chamber Group at UCRL, for his advice and encouragement; to Drs. Robert D. Tripp and Arthur H. Rosenfeld for their assistance and suggestions during the preparation and execution of the experiment; to Dr. Frank Solmitz for his guidance throughout the entire project; and to the bubble chamber operating crew.

This work was done under the joint auspices of the United States Naval Postgraduate School and the United States Atomic Energy Commission.

TABLE OF CONTENTS

TABLE OF CONTENTS

LIST OF ILLUSTRATIONS

LIST OF ILLUSTRATIONS

TABLE OF SYMBOLS AND ABBREVIATIONS

D	The distance on the film between the two stereo images of the same space point.
e	Particle of electronic mass ≈ 0.51 Mev.
E	Kinetic energy of a particle
f	Demagnification constant in the optical system of the bubble chamber
H	In the optical system of the bubble chamber, the distance from the camera lens to the top of the chamber
K	K meson (mass ≈ 965 electron masses)
k	Magnification constant in the bubble chamber optical system
L	True length of particle path in matter, length of chord of a circle
m	Mass of a particle
N	Number of atoms per cubic centimeter; number of events
P	Pressure in atmospheres or lb per in.^{2}
q	The effective distance from the camera lens to the film in the bubble chamber optical system
r	Radius of curvature
R	Residual range of a particle in matter
s	Length of an arc of a circle
S	Entropy
T	Temperature in degrees Kelvin
v	Specific volume in cm^3 per mole
x, y, z;	Coordinates of a point in the bubble chamber
X^I, Y^I	Coordinates of a point in View I of the stereo pair of bubble chamber pictures
X^{II} Y^{II}	Coordinates of a point in View II of the stereo pair of bubble chamber pictures
δ	Horizontal distance between the optical axes of the camera lenses in the bubble chamber optical system
ν	Neutrino, neutral particle of mass ≈ 0
Λ^0	Neutral unstable particle of mass ≈ 1114 Mev ≈ 2228 electron masses

λ	Angle of dip from horizontal of a track in bubble chamber
ρ	Density in g per cm^3
π	Pion or π meson, particle of mass $\approx$ 270 electron masses
μ	Muon or μ meson, particle of mass $\approx$ 200 electron masses
τ	Mean lifetime
θ^0	Neutral unstable particle of mass $\approx$ 965 electron masses
θ	Angle subtended by chord 1
θ_i^2	Mean square angle of scatter
Ξ	Hyperon of mass $\approx$ 1190 Mev $\approx$ 2380 electron masses
H_2	Molecule of hydrogen
D_2	Molecule of deuterium
HD	Hydrogen deuteride
psia	lb per $in.^2$, absolute
psig	lb per $in.^2$, gauge
^oK	Temperature in Kelvin or absolute scale
Mev, Bev	Million, billion electron volts, ; mass or energy units
$\frac{dE}{dx}$	Stopping power of a substance
$\frac{dR}{dz}$	Variation of residual range of a particle with depth in the bubble chamber
$\frac{d\rho}{dz}$	Variation of density of liquid hydrogen with depth in the bubble chamber

$\frac{dE}{dx}$	Ionization energy loss per unit path length
$\frac{dE}{dt}$	Variation of rotational energy of a particle with respect to the inertial observer
$\frac{dn}{dx}$	Variation of refractive index of [illegible] per unit length in the inertial observer

1. Introduction

Since the first successful operation of a bubble chamber by Glaser [1] in 1952, its use as an instrument for nuclear research has grown rapidly and the information yielded has aided our understanding of nuclear physics. At the present time various types of chambers are in use or under development. These differ in many respects, but primarily they can be classified by the type of sensitive material used, i.e., hydrogen, hydrocarbons, or--more recently--helium. The advantages and disadvantages of using hydrogen as the active material are fully discussed elsewhere [2]. At the University of California Radiation Laboratory a 10-inch hydrogen bubble chamber is being used in the study of the production and decay of short-lived unstable particles such as $K^{\pm}$, θ^0, Λ^0, and $\Sigma^{\pm}$. An accurate range-energy relation is needed in determining the kinematics of the processes involved. If the density of the liquid hydrogen were known, one could use the Bethe-Bloch theory [3, 4] to determine the range-energy relation. It is, however, very difficult to measure the density of superheated liquid hydrogen, the condition in which it is sensitive to ionizing particles, because it remains in this condition only 20 to 30 msec. One could extrapolate into the superheated region, using measurements made on the normal liquid, but the accuracy of this method is unsatisfactory for studies of the unstable particles mentioned above.

One point on the range-energy relation can be found if we measure the range of a particle of known initial and final kinetic energy. Using this experimental point we can calculate the density of hydrogen for use in the Bethe-Bloch theory to determine the range-energy relation over a wide range of energies.

The method selected for the experimental determination of a point on the range-energy curve was to measure the range of the μ^+ meson in the $\pi^+ \rightarrow \mu^+ \rightarrow e^+$ decay chain. The selection was based on such factors as the accuracy with which the μ^+ energy is known, the accuracy with which the μ^+ range could be measured, and the

availability of π^+ mesons in sufficient quantity and at the proper energy range.

The predominant mode of decay of the π^+ meson is $\pi^+ \rightarrow \mu^+ + \nu$. Experimental evidence for other modes of decay for the π^+ exists [5], but the branching ratios are so small ($\sim 10^{-4}$ to 10^{-5}) that for our purposes the decay of the π^+ can be considered a two-body decay yielding a μ^+ with 4.12 ± 0.02 Mev [6] initial kinetic energy if the decay takes place at rest.

The μ^+ is known to decay at rest according to the relationship

$$\mu^+ \rightarrow e^+ + \nu + \nu.$$

The e^+ has a finite energy spectrum, because the decay involves more than two products. The important feature of the μ^+ decay is that it does take place at rest, i.e. at zero kinetic energy, and is evidenced by the formation of the positron. Knowing the initial energy of the μ^+, we need only measure its range in the bubble chamber to obtain a point on the range energy curve, and as explained above, the range-energy relation. In the actual extrapolation of the range-energy relation from the point determined to other energies it is simpler to use the data on protons available in the literature. Aron [7] has computed range-energy tables for protons in hydrogen at standard conditions. These tables are based on a theoretically determined mean-excitation potential of 17.5 ev [8] for hydrogen. By properly scaling the data we can calculate the range-energy relation for hydrogen under the operating conditions of the bubble chamber.

Since the kinetic energy of the μ^+ at the time of its formation is known to only ±1/2 % [6], a final range error of ±1/3% seemed a reasonable objective. The factors affecting the final range error are range straggling and measurement errors. If measurement errors can be made small compared to the range straggling, the accuracy of our range determination will be limited by the number N of μ^+ ranges measured, i.e.,

$$\text{range error} \cong (\text{straggling} + \text{measurement error})/N^{1/2} .$$

Then for a measurement plus straggling error of 5%, we need to measure about 300 μ^+ ranges to reduce our range error to 1/3%.

To minimize the measurement errors, certain restrictions in the selection of $\pi^+ \rightarrow \mu^+ \rightarrow e^+$ events for measurement had to be observed. Since tracks in the chamber consist of a series of bubbles separated by finite distances, one cannot assume that the first and last bubble in any series marks the beginning and end of the particle track. In $\pi^+ \rightarrow \mu^+ \rightarrow e^+$ decay events, the points of intersection between the π and the μ and between the e and the μ determine the limits of the μ travel. These points of intersection, once determined, offer the easiest method of measuring the length of the μ track. The error in the determination of a point of intersection is inversely proportional to the sine of the angle of intersection, and both angles of intersection enter into the final range accuracy.

As may be seen in Fig. 1, the stereo angle of the camera used with the 10-inch bubble chamber is $\sim 4^\circ$. This small angle makes measurement errors sensitive to the error in depth determination. Specifically, the error in range is proportional to the product of the error in the measurement of change in depth of the particle track, and the sine of the angle of dip of the particle track, i.e. measurement error = (error in Δz) sin λ .

Finally, an error in the measurement of range may be introduced by π^+ mesons that decay in flight but cannot be recognized as doing so. On the basis of a π^+ lifetime of $\tau = 2.56 \times 10^{-8}$ sec [9], the probability of decay in flight in the last centimeter of range is calculated to be 0.0076. This error is obviously insignificant. The μ^+, being much longer-lived [9] that the π^+, has a correspondingly smaller chance to decay in flight.

With the range-energy relation determined, and the density of the superheated liquid hydrogen calculated, we can comment on the advisability of extrapolating the known data on normal liquid hydrogen into the superheated region.

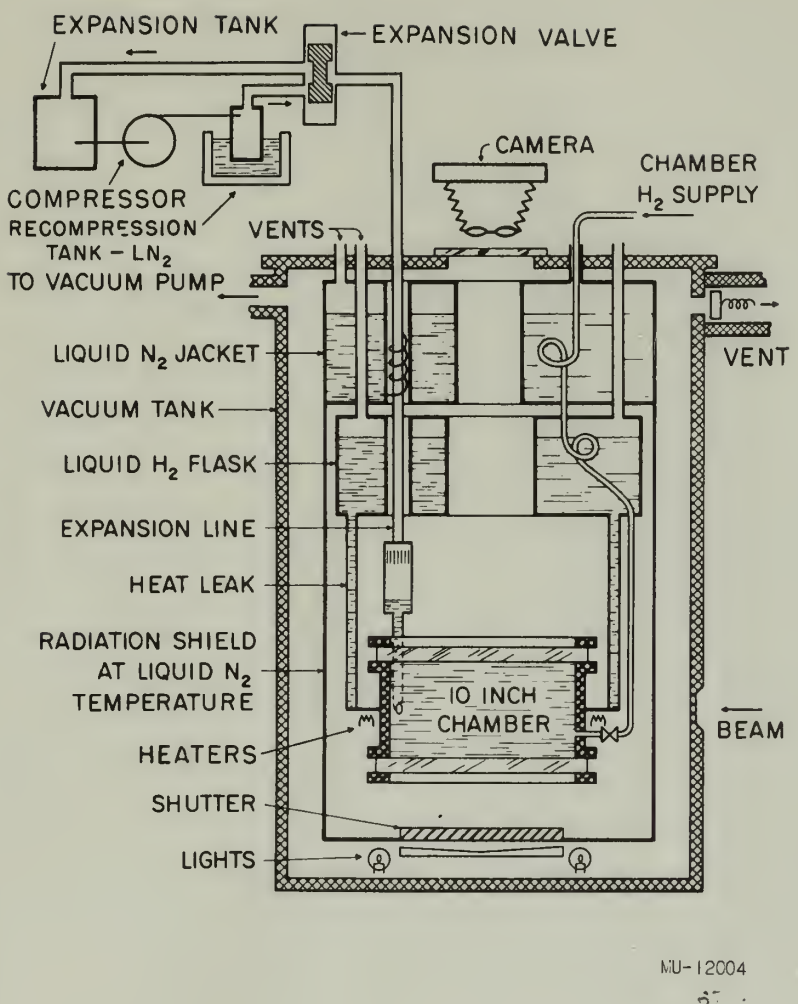

Fig. 1. Line drawing of 10-inch hydrogen bubble chamber

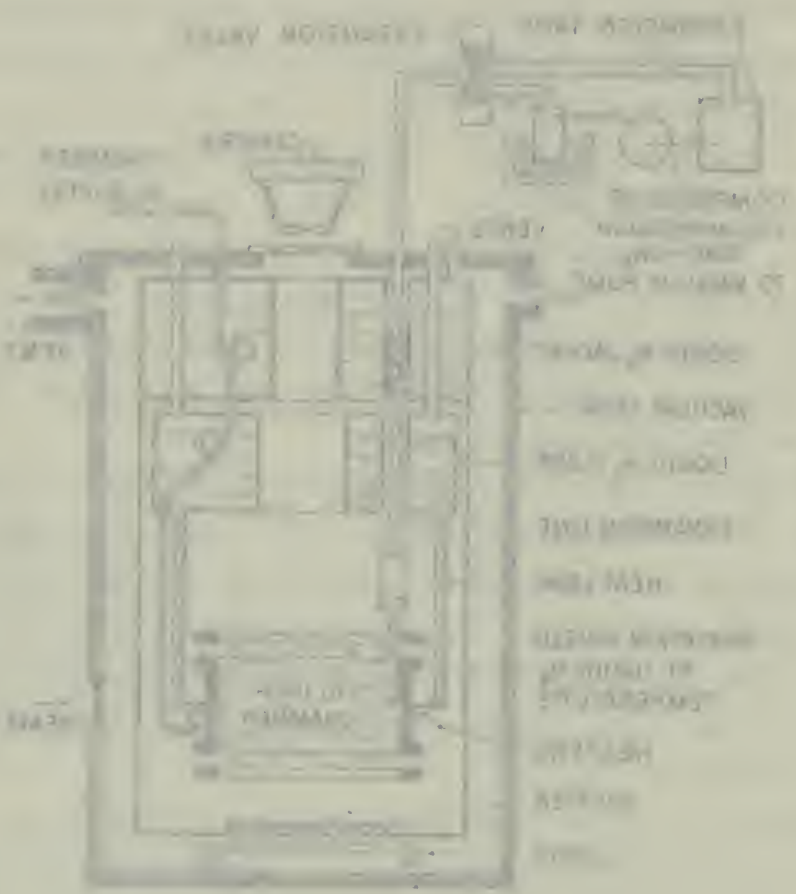

2. Experimental Arrangement

The π^+ beam was obtained by bombarding the 79° lead target of the Bevatron with protons of 3 Bev energy; π^+ mesons of approximately 245 Mev/c momentum were emitted in the backward direction and deflected out through the 76° window by the Bevatron magnetic field. A small "C" magnet placed at the exit window was used to make minor corrections in the directions of the π^+ beam. After being focused by a 4-inch quadrupole magnet, the beam was deflected through 60° and collimated into a 4-by-4-inch cross section for entry into the 10-inch bubble chamber. The quadrupole-magnet current was adjusted to focus the beam at the bubble-chamber-entrance window. A schematic of the experimental arrangement is shown in Fig. 2.

To stop the π^+ mesons in the center of the chamber, the beam momentum had to be reduced from 245 to 120 Mev/c prior to entry of the beam into the vacuum jacket surrounding the chamber. The value 120 Mev/c takes into consideration the stopping power of the vacuum jacket, the chamber window, and 5 inches (chamber radius) of liquid hydrogen at a density of about 0.06 g/cm^3. The true energy of the π^+ beam was determined by taking a range curve with copper as the absorber. The Bevatron beam intensity was 2×10^9 protons per pulse. This was calculated to give an average of three π^+ per pulse stopping in the chamber. Some of the pulses yielded many more, as shown in Fig. 3.

Although the chamber was surrounded with lead shielding, it was necessary to turn on the bubble chamber magnet to reduce the background of low-energy particles, mostly electrons, entering the chamber and obscuring the decay events. The curvature of charged-particle tracks caused by the magnetic field of the chamber introduces a systematic error in the range measurements. The error introduced was found to be insignificant (see discussion of magnetic curvature in Section 5E).

4. Experimental Investigation

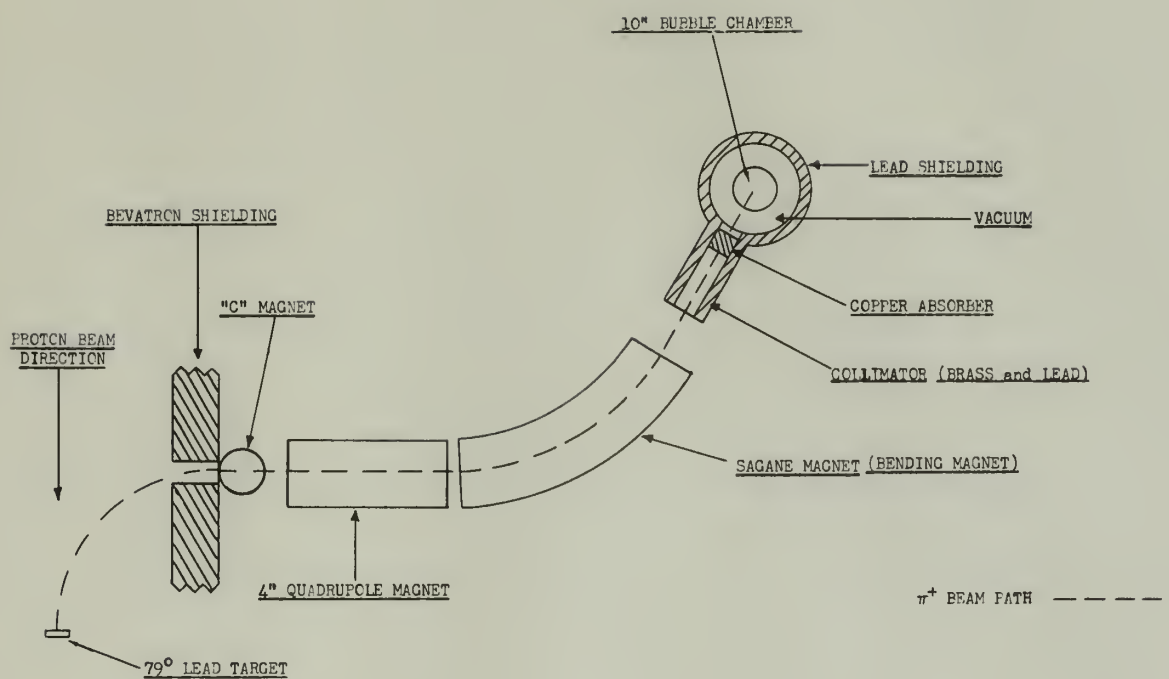

Fig. 2. Experimental arrangement

ZN-1707

Fig. 3. Photograph of $\pi^+ \rightarrow \mu^+ \rightarrow e^+$ tracks in the 10-inch bubble chamber

Locating, positioning, and focusing the beam was done by use of coincidence techniques with scintillation counters. Background effects were reduced by gating the scalers to count only during the Bevatron pulse.

3. Measurement of Liquid Hydrogen Temperature and Pressure

A. Temperature

Temperature measurements in the 10-inch bubble chamber are made with two hydrogen-filled vapor-pressure thermometers whose bulbs are located one above the other about 3.6 inches apart on the inside wall of the chamber (see Fig. 4). The bulbs are connected to opposite sides of a pressure-difference gauge located outside the chamber. This gauge provides a means for measuring the vertical temperature gradient during the operation of the chamber. The lower of the two bulbs is also connected to a Bourdon pressure gauge.

During chamber operation the temperature is automatically controlled with heaters surrounding the chamber wall [10]. The pressure in the lower bulb is used in the controlling. The desired chamber temperature is preset on the controller, and this temperature is maintained within the accuracy of the Bourdon Gauge ($\pm$ 0.2 psig = $\pm$ 0.02 ^{o}K at 65.5 psig). The vapor-pressure difference varies slightly during operation. The chamber temperature was checked continuously and recorded at least once every 5 to 10 minutes during the 3 hours the experiment lasted. The reading of the lower vapor-pressure thermometer remained essentially constant, and equal to the value set on the Bourdon Gauge. According to the experimentally determined vapor-pressure curve for liquid hydrogen [11], the 65.5-psig reading of the lower thermometer is equivalent to 27.8 ^{o}K, and the average vapor-pressure difference of 3.5 psi corresponds to a temperature gradient of 0.021 ^{o}K/cm.

B. Pressure

The problem of determining the pressure to which the hydrogen expands was far more difficult than the temperature measurements. Built

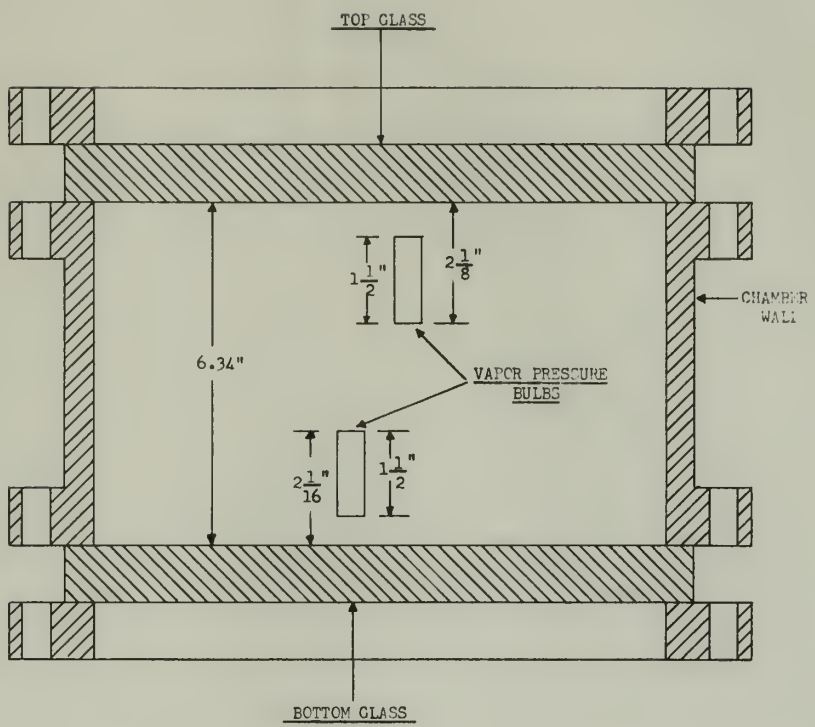

Fig. 4. Sketch of vapor-pressure-temperature bulbs in the 10-inch bubble chamber

into the walls of the chamber is a pressure-sensing device referred to locally as a Linlor pressure gauge [12]. The gauge gives an indication of the instantaneous pressure in the chamber, and is used primarily in adjusting the bubble chamber operating cycle. The gauge basically operates as follows: a change in pressure in the chamber causes a change in capacitance in an electrical circuit, which is converted into a change in voltage and displayed on an oscilloscope. In principle the method is quite simple, and the gauge accomplishes the purpose for which it was designed. However, the gauge does have certain limitations that could not be eliminated. The limitations were: (a) the sensitivity of the gauge was very low, (b) the reference voltage of the gauge as well as the sensitivity was subject to drift, and (c) the response of the gauge was nonlinear.

The pressure measurements were made in the following way. With each Bevatron pulse, the voltage output signal from the Linlor gauge was displayed on an oscilloscope. The oscilloscope screen was monitored continuously, and a series of pictures taken every 5 to 10 minutes to correspond with temperature measurements. Land camera pictures gave better results than a 35-mm scope camera. A typical picture of the pressure cycle is shown in Fig. 5.

While the bubble chamber was warming up to its pre-expansion condition at 27.8°K and 70 psig, the Linlor gauge was calibrated by simultaneously recording the actual chamber pressure at 5-psig intervals as indicated on the Bourdon gauge, and photographing the voltage output on the scope for later measuring on a traveling microscope. Calibration data were also taken while the chamber was being cooled down at the end of the experiment. Data were also collected on other days in order to obtain some knowledge of the kind and amount of drift in the Linlor gauge. All the data, when analyzed, provided a reasonably good calibration curve of chamber pressure versus pulse height.

The photographs of the Linlor-gauge output voltage taken during the experiment provided a measure of chamber pre-expansion and post-expansion pressure. With each photograph that was taken the actual

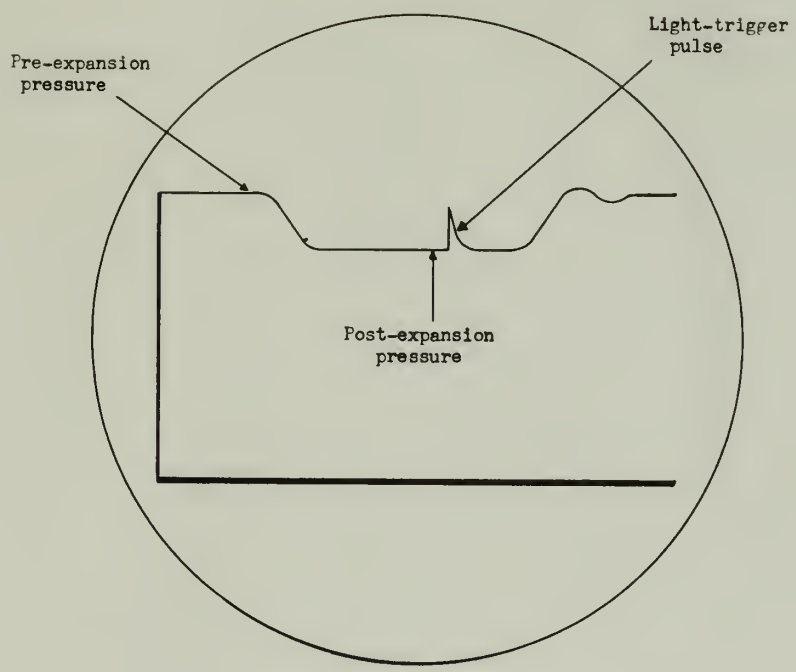

MU-13396

Fig. 5. Oscilloscope photograph and sketch of chamber pressure variation during expansion

pre-expansion pressure was read from the Bourdon gauge, and comparison of this pressure with the pulse height gave a measure of the Linlor-gauge drift for that particular chamber cycle. If the pre-expansion pressure and its corresponding pulse height did not fall on the calibration curve, the readings were normalized by use of the previously obtained knowledge of drift. After normalization of the reading, the postexpansion pulse height as measured on the picture was applied to the calibration curve, and the corresponding pressure obtained.

The value of the postexpansion pressure during the entire experiment was 48 ± 5 psia.

4. Thermodynamics of the Expansion

As was mentioned in the section on temperature and pressure measurements, the pre-expansion and postexpansion pressures are known by direct measurement. The pre-expansion temperature is also known. The expansion of the liquid takes place in about 10 milliseconds, and therefore if there is a change in temperature during expansion it is not registered on the vapor-pressure meter, since the time constant of the meter and associated system is many times as large. There are two possibilities of importance; the expansion is either isothermal or adiabatic. The question of which process is correct was not answered experimentally, but has been calculated theoretically by solution of the boundary-value problem of heat transfer from the walls of the chamber to the liquid in the chamber [13]. The results show that the time for the temperature difference between the wall and the center of the chamber to drop to 1/e of its initial value is approximately 2 hours. The effects of convection were neglected in this calculation. The characteristic time involved in convection phenomena is certainly less than 10 milliseconds, otherwise there would be large track distortions in the chamber. This provides rather convincing proof that the expansion is adiabatic.

Knowing the expansion to be adiabatic, we can determine the postexpansion temperature of the liquid hydrogen. This, however, requires extrapolation from the liquid region into the superheated liquid region, using the latest appropriate experimental data on liquid hydrogen.

Johnston, Keller, and Friedman [14] found that on a P-T diagram the isochores (lines of constant volume) are, within experimental error, straight lines. Therefore extrapolation seems quite reasonable.

The ratio of the adiabatic change of density with pressure to the isothermal change of density with pressure is equal to the ratio of c_v and c_p, i.e.,

$$\frac{(\partial\rho/\partial P)_S}{(\partial\rho/\partial P)_T} = \frac{c_v}{c_p} .$$

Extrapolating the data of Eucken [15] and Gutsche [16] as summarized in NBS Report No. 1932 [17] into the superheated region gives 3.2 cal/mol-^{o}K and 9.4 cal/mol-^{o}K for the values of c_v and c_p, respectively. This gives a ratio of 0.34. Using the pre-expansion values of $T = 27.8^{o}K$ and $P = 70$ psig and the data of Johnston et al. [14], one finds the post-expansion temperature of the liquid hydrogen to be $27.5 \pm 0.1^{o}K$ (a temperature drop of $0.3 \pm 0.1^{o}K$).

As was seen earlier, the pressure in the chamber is known to considerably less accuracy than the temperature. To see what the relative importance of these two quantities is in determining the density of the hydrogen one can find the ratio

$$\frac{(\partial\rho/\partial T)_P}{(\partial\rho/\partial P)_T} = -\left(\frac{\partial P}{\partial T}\right)_\rho .$$

Johnson et al., [14] have represented their data with the empirical equation,

$$P = A(\rho) - 7.11\ T + 437\ \rho T ,$$

where P is in atmospheres, ρ in mol/cm^3, T in ^{o}K, and A is a function of ρ only. Using this equation to determine $(\partial P/\partial T)_\rho$ at

$T = 27.5^{\circ}K$ and $P = 48$ psia, one obtains

$$\frac{(\partial\rho/\partial T)_P}{(\partial\rho/\partial P)_T} = -5.7 \frac{\text{atm}}{^{\circ}K} = -83.8 \frac{\text{psi}}{^{\circ}K} .$$

Since our temperature measurements are accurate to $0.1\ ^{\circ}K$ and our pressure measurements to 5 psi, we find the percentage error in density caused by the temperature error to be twice the percentage error caused by the pressure-measurement error. This then shows that the temperature is the thermodynamic variable that is more important in determining the accuracy of the density.

It was pointed out in the section on temperature measurements that there existed in the chamber a temperature gradient. With an average vapor pressure difference of 3.5 psi ($0.2^{\circ}K$), assuming the temperature gradient to be linear, we obtain a density gradient of

$$d\rho/dz = 0.000059\ g/cm^3/cm$$

and a percentage range gradient of

$$(dR/R)/dz = 0.10\%/cm .$$

This gives a 1.6% change in range from top to bottom of the chamber. The effect of this on the average range of μ^+ mesons in the chamber is to give a somewhat larger standard deviation than that caused by the 3.3% expected range straggling.

It should be pointed out that the data of Johnston et al. [14] are for liquid normal hydrogen (25% para-75% ortho). In the bubble chamber the liquid hydrogen differed in two respects. It was parahydrogen (99.70% para-0.21% ortho), and it contained a trace of deuterium. The content was as follows:

$$H_2 = 99.03\%, \quad HD = 00.91\%, \quad D_2 = 00.06\%,$$

Neglecting the D_2 content, the ratio of the range in parahydrogen to the range in the above mixture at the same conditions is dependent on the ratio of the specific volume of hydrogen to the specific volume of hydrogen deuteride in the following way:

$$R_{H_2} / R_{HD} = \frac{1 + (\%HD/\%H_2)\,(V_{H_2}/V_{HD})}{1 + (\%HD/\%H_2)} .$$

Using the data from NBS Report 1932 [17], one finds this ratio to be

$$R_{H_2} / R_{HD} = 1.0009 \pm 0.0006 .$$

Since this range error introduced by ignoring the deuteride content amounts to $0.1 \pm 0.1\%$ of the final range, we considered it insignificant, and did not include it in arriving at our final results.

5. System of Measurement of the μ^+ Meson Track Length

A. General

As illustrated in Fig. 1, 35-mm stereo pair pictures were taken from above the bubble chamber. After it was developed, the film was scanned quickly for events of interest, in this case, $\pi^+ \rightarrow \mu^+ \rightarrow e^+$ decay chains. This initial scanning enabled us to eliminate those events which by their appearance in two dimensions obviously involved decay in flight of the π^+, or which by their orientation in the chamber could not be measured to the degree of accuracy desired. Those events which were not eliminated in this initial scanning were measured on a precision projection microscope developed at UCRL and shown in Figs. 6 and 7. The microscope projects the 35-mm pictures containing the events onto a viewing screen. The coordinates of any point in the pictures can be measured and punched automatically on IBM cards. This allowed us to store the coordinates of successive points along the tracks of π^+, μ^+, and e^+ particles on the cards, which when programmed into an IBM computer enabled us to determine the range of the μ^+. The entire process is discussed in the following sections.

ZN-1706

Fig. 6. Front view of projection microscope

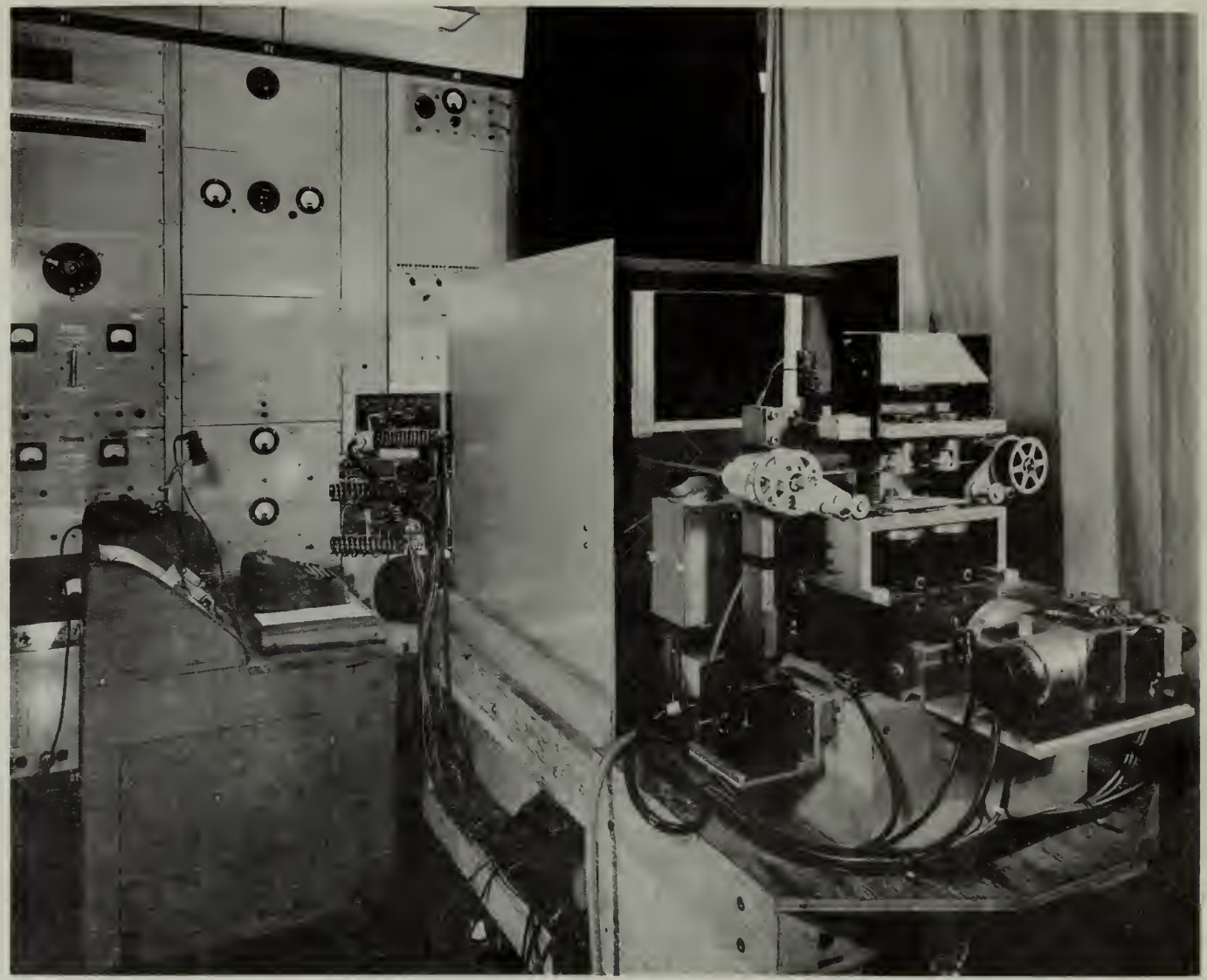

ZN-1705

Fig. 7. Rear view of projection microscope

B. Precision Projection Microscope

The precision projection microscope shown in Figs. 6 and 7 projects the film pictures onto a large screen. The microscope table on which the film is placed is provided with independent x and y motions accurately determinable to the nearest micron. The position of the microscope table is transferred to IBM cards, using a Wang digitizer [18] and a standard IBM card-punch console. A fixed cross hair is also projected onto the screen and used in measuring points along the various particle tracks. The track length used for the π and e was approximately one and a half times the length of the μ track. Seven to 12 points along each track were recorded on the cards in a definite sequence to simplify the computer program. The order in which tracks were measured is shown in Fig. 8.

C. Solution of Optical Problem

The space coordinates of a point in the chamber are obtained from the film coordinates by multiplying the film x and y coordinates with an appropriate magnification constant as follows (see Appendix I for details of the space construction):

$$x = kX^I , \qquad y = kY^I , \qquad z = kq .$$

For a perfect optical system, the magnification constant k should be constant throughout any z plane, and be dependent on the horizontal lens separation (δ) and the film coordinates of the point:

$$k = \delta/(X^I - X^{II}) .$$

The differences between the x, y, and z coordinates of two points in the chamber would then be

$$\Delta x = k_1 X_1^I - k_2 X_2^I ,$$
$$\Delta y = k_1 Y_1^I - k_2 Y_2^I ,$$
$$\Delta z = (k_1 - k_2) q .$$

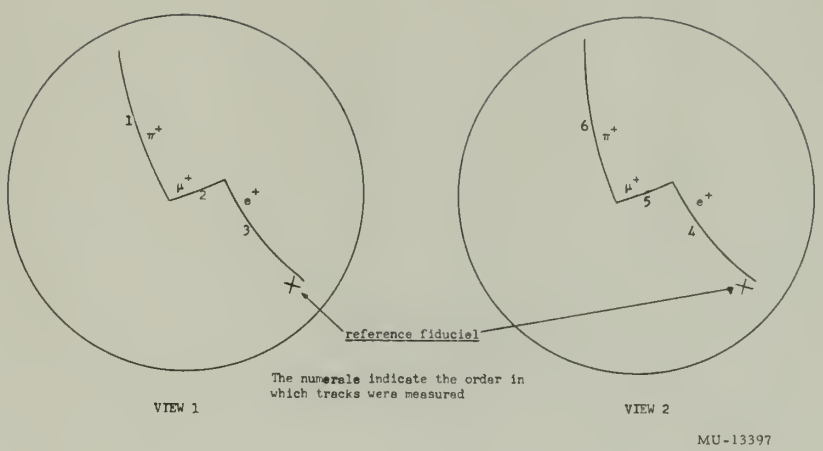

Fig. 8. Schematic of stereo picture of bubble chamber showing the order of measurement of $\pi \rightarrow \mu \rightarrow e$ events

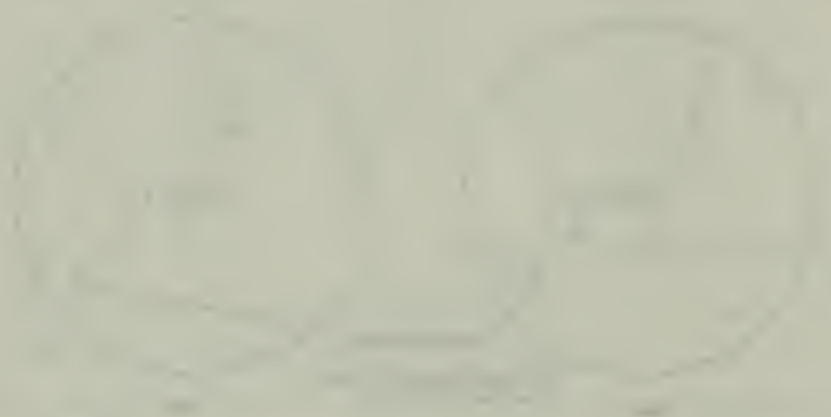

The preceding remarks and those in Appendix I on the solution to the bubble chamber optical problem have been greatly simplified. Some of the complicating effects encountered and the methods used to correct or eliminate them should be mentioned. To determine k and δ, we had to measure on the film the distances between the images of reference fiducial marks permanently inscribed in the top and bottom glass. Then we compared these film distances to the known space distances between the fiducials. The results of these measurements required us to accept a different magnification for the x and y directions in any one z plane and a different magnification in each stereo view, or a total of four magnification constants for any one point. The need for these different magnification constants can be explained as the result of uneven shrinkage of the film during development, differences in the adjustments of the two lenses, and a preset 1.5° tilt of the chamber from the horizontal to prevent the accumulation of bubbles at the top glass. We added all the observed systematic variations in the optical system, and corrected for them by using different magnifications for each view and each coordinate direction within the view.

D. Computer Program

The problem of calculating the range of the μ^+ was programed for the IBM type 650 computer. Essentially the computer determined a least-squares parabola to fit each track in both views, and determined the points of intersection between the parabolas representing the π^+ and μ^+ tracks and the μ^+ and e^+ tracks in each view.

It is true that the track of a particle stopping in a magnetic field is not a parabola. But, weighing the ease of programing the problem for a parabola (as compared with a higher-order curve) against the required accuracy of measurement, we selected the parabola. Once the four points of intersection in the film were determined, it was a simple matter to have the computer determine the distance between the two intersections in space, as outlined in the section on the optical problem, as well as any other information desired about angles of intersection, average depth

of the μ^+ in the chamber, etc. To improve the over-all accuracy of the measurements, provision was made in the computer program to eliminate any event in which the coordinates of the last measured point at the end of a track was more than 9 microns off the least-squares parabola fit.

E. Systematic Corrections to Measured Range

We wish to determine the difference in length between the actual curved path (s) of the μ^+ in the bubble chamber, and the straight-line-approximation (L) to the path calculated with the computer program. The approximate range-momentum relation

$$s = \alpha p^{3.66} \tag{1}$$

can be expressed in terms of the radius of curvature r in a magnetic field as

$$s = \beta r^{3.66} \tag{2}$$

if the path of the μ^+ is perpendicular to the magnetic field. To express this equation in x and y coordinates we use the parametric equations

$$r = \frac{ds}{d\tau} \; ; \quad \sin \tau = dy/ds; \quad \cos \tau = dx/ds \; , \tag{3}$$

where τ is the angle that a tangent to the particle path makes with the x axis. On substituting Eqs. (3) into (2) and using the relationship $ds = 3.66\beta r^{2.66} dr$ obtained by differentiating Eq. (2), we obtain

$$\tau = \frac{3.66\beta}{2.66} r^{2.66} \; , \tag{4}$$

$$dy = \sin \left(\frac{3.66}{2.66}\beta r^{2.66}\right) \; 3.66\beta r^{2.66} dr, \tag{5}$$

$$dx = \cos \left(\frac{3.66}{2.66}\beta r^{2.66}\right) \; 3.66\beta r^{2.66} dr. \tag{6}$$

Expanding the sin and cos terms in Eqs. (5) and (6) and performing the indicated multiplication, we obtain an infinite series. This series is convergent in the region of interest, that is, for particles of initial kinetic energy less than 5 Mev. Integrating the series term by term and summing significant terms, we can determine x and y accurately to four decimal places. We can then calculate $L = (\Delta x^2 + \Delta y^2)^{1/2}$ and solve for $\frac{s-L}{s}$, that is, the percentage difference between the length of the curved path and the straight-line approximation.

We find this percentage difference to be 0.08% for the μ^+, and have ignored it in arriving at our final results.

The mean range (R) as measured is not the true range (L) of the particle given by the Bethe-Bloch [3,4] theory. Because of multiple scattering, the measured range is shorter than the actual path length. To obtain an approximation of the difference between these two values, consider the particle path to be broken up into small segments dL, and the projection of these on the beam direction to be dR. Then we have

$$dR = dL \cos \theta_i ,$$

where θ_i is the angle of scatter. Since we are considering small-angle scattering only, this gives

$$dR = dL \left(1 - \frac{\theta_i^2}{2}\right) .$$

Using the approximation by Segrè [19] for the mean square angle of scatter, we have

$$dR = dL - m_e/m_\mu \ln (E_0/E_i) \frac{dL}{2} ,$$

where E_0 is the initial energy and E_i is the final energy of the μ meson. With the approximate range-energy relation $R = a E^{1.83}$, we have integrated the above equation to obtain $\frac{L - R}{L}$. The correction thus obtained is 0.1%. The value of range given in the results has been corrected by this amount.

6. Results and Conclusions

During the experiment about 1400 stereo pair pictures were obtained. These yielded approximately 3000 $\pi^+ \rightarrow \mu^+ \rightarrow e^+$ decay events in the chamber. During preliminary scanning we attempted to select for measurement only those events in which the angles of intersection of the particle tracks were between 30° and 150°. In addition, all events in which the μ^+ track appeared to dip more than 45° were discarded because of the large error inherent in the measurement of steeply dipping tracks. We were left with 771 events, which were measured on the precision projection microscope previously described. The computer program was designed to give not only the range of the μ^+ but also its dip and the angles of intersection of the tracks. Of the 771 events measured, 327 had a μ^+ dip angle greater than 30°, and were discarded as being subject to too large an error. A histogram of the remaining 444 events is shown in Fig. 9. Superimposed on the histogram is a normal distribution curve showing the average value of the range equal to the arithmetic mean of the 444 events and the standard deviation equal to that obtained from them.

Taking the arithmetic mean as the most probable value, we obtained a range of 1.102 ± 0.003 cm with a standard deviation of 0.055 cm (5.0 %) for the μ^+ in liquid parahydrogen. The correction for multiple scattering gives 1.103 ± 0.003 cm. This value corresponds to a z plane 7.1 cm from the top of the chamber, which is 16 cm deep. Using the range tables of Aron, [7], which are based on the Bethe-Bloch theory, we obtained the range-energy curves shown in Fig. 10.

Using the compilation by Crowe [6] for rest mass and the initial energy of the μ^+ meson ($E = 4.12 \pm 0.02$ Mev and $M_{\mu^+} = 206.86 \pm 0.11\, m_e$), and the range tables of Aron [7], we obtained 0.0583 ± 0.0006 g/cm^3 for the density of superheated liquid parahydrogen at $27.6 \pm 0.1^\circ$K and 48 ± 5 psia. The density under the same conditions for liquid normal hydrogen is calculated as 0.0591 g/cm^3 from Johnston's data [14], and 0.0587 g/cm^3 from Kammerlingh Onnes' data [20]. It should be emphasized

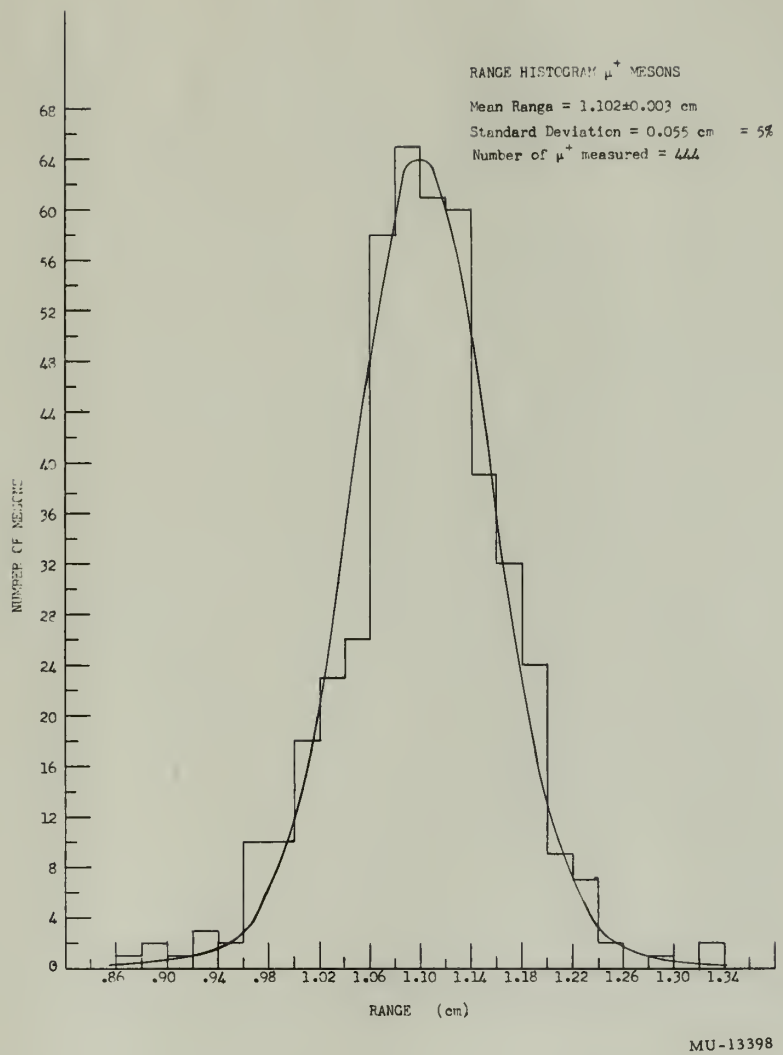

Fig. 9. Range histogram of 4.12-Mev μ^+ mesons in liquid hydrogen

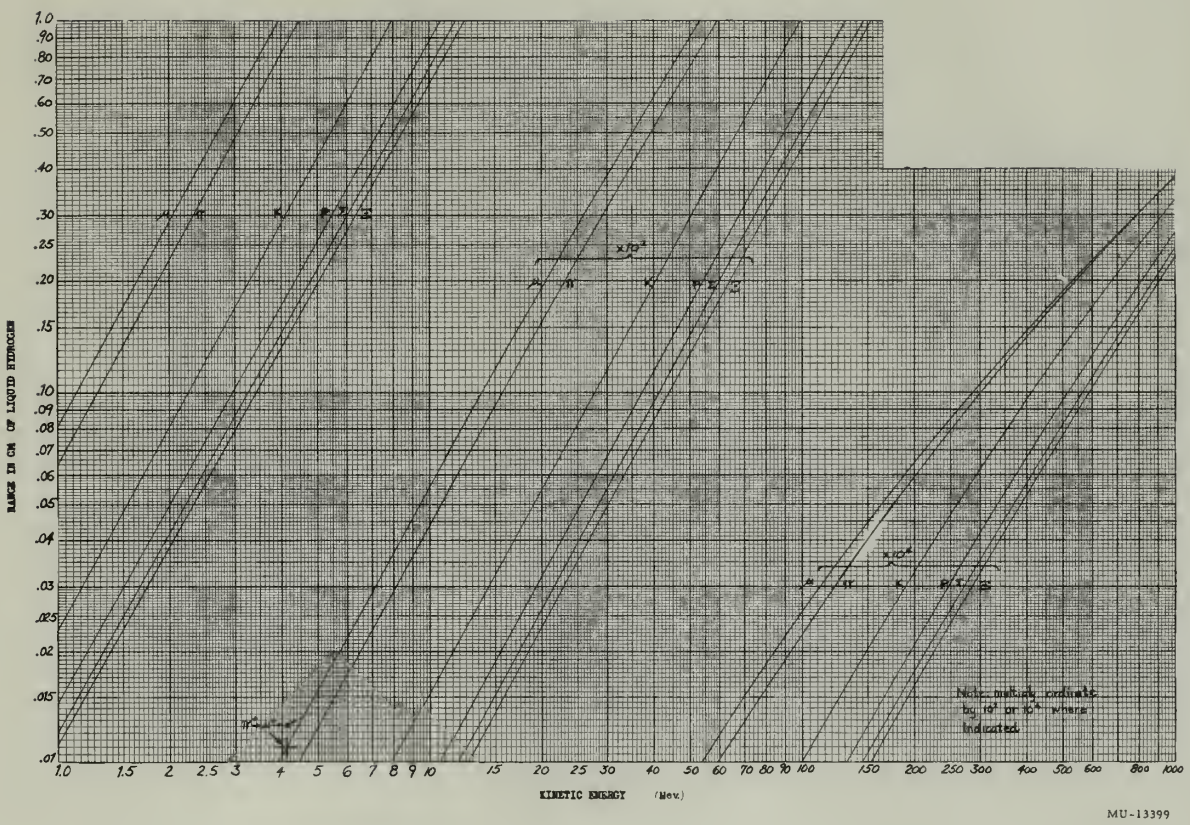

Fig. 10. Range-energy curves in liquid H_2 bubble chamber based on experimentally determined range of 1.103 ± .003cm for μ^+ from π^+ decay.

Liquid H_2 conditions: T = 27.6 ± 0.1 °K;
P = 48 ± 5 psia; $\rho = (5.83 \pm 0.06) \times 10^{-2}$ g/cm^3

Following mass ratios used:
$M_\mu/M_p = 0.1127$; $M_\pi/M_p = 0.1488$; $M_k/M_p = 0.526$
$M_\Sigma/M_p = 1.270$; $M_\Xi/M_p = 1.408$

that the latter two values are for normal hydrogen and that our value is for parahydrogen. Since the value of Johnston et al. [14] differs by only about 1%, we consider that their data extrapolated into the superheated region are adequate for bubble chamber thermodynamics and engineering purposes.

Since there should be a vertical gradient in the chamber, we were interested in examining the correlation, if any existed between the range of the μ^+ and its depth in the chamber. Using only those events (228) in which the μ^+ track is very flat, 0° to 15° dip, we obtained a value of -0.14 for the correlation coefficient and determined the slope of the regression line of range on depth to be -0.002 cm/cm. This value compares favorably with that calculated by use of the temperature gradient observed and the data of Johnston et al., [14] which gave -0.001 cm/cm. The value obtained from correlation theory has a very large uncertainty, but does show that there is a variation of the range with vertical position in the chamber. It also points out that for particles that experience little straggling, the vertical position of the track should be taken into account when the energy is being calculated from residual range measurements.

We have calculated the theoretical straggling by integrating numerically the expression given by Bohr [21],

$$\left\langle (R - R_0)^2 \right\rangle \text{ ave.} = 4\pi e^4 NZ \int_0^{E0} (dE/dx)^{-3} = 3.2\%,$$

for the 4.12-Mev μ^+ meson in liquid hydrogen. The value obtained is that amount of straggling caused by collisions with electrons only. Toward the end of the μ^+ track nuclear collisions would become important and give rise to a larger value. We have estimated our measurement error to be 2.5%, which with the 5% standard deviation obtained experimentally gives a straggling of 4.3%. We believe that this value represents a good estimate of the actual straggling of the 4.12-Mev μ^+ mesons in liquid parahydrogen.

APPENDIX I

Solution to the Optical Problem

Constants. Figure 11 is a diagram of the bubble chamber camera optics. No attempt was made to draw it to scale. For comparison purposes $H = 100$ cm, $\delta = 9$ cm, $q = 10$ cm. C is the center of the top glass of the chamber, D is the distance between the images of the chamber center as seen in the stereo pair. AF and A'F' are the optical axes. From geometrical considerations, we have

$$AC/H = d/q \quad \text{and} \quad CA'/H' = d'/q'; \tag{A.1}$$

assuming $H = H'$, and $q = q'$, we define the magnification in the plane of the top glass as $k = H/q$. (A.2)

Substituting Eq. (A.2) in (A.1), we obtain

$$AC = (d/q)H \quad \text{and} \quad CA' = (d'/q)H;$$

then

$$AC + CA' = \delta = (H/q)(d + d')$$

$$\delta = k(D - \delta)$$

$$\delta = D/(1 + 1/k).$$

We can determine D and k directly from the film and then calculate δ. With these constants determined we can proceed to a determination of the coordinates of any point in the chamber from the stereo pair of pictures.

Range Measurements in the Chamber. In the following refer to Fig. 11. Point A is the assumed origin of coordinates in the bubble chamber, x, y, and z represent bubble chamber coordinates of point P, and X_1^I, Y_1^I, X_1^{II}, Y_1^{II} are the corresponding film coordinates (subscripts denote point number, superscripts denote view number). The origin of the film coordinates is the projected optical axis in each view; positive X direction is to the right in the figure. We have the film coordinates

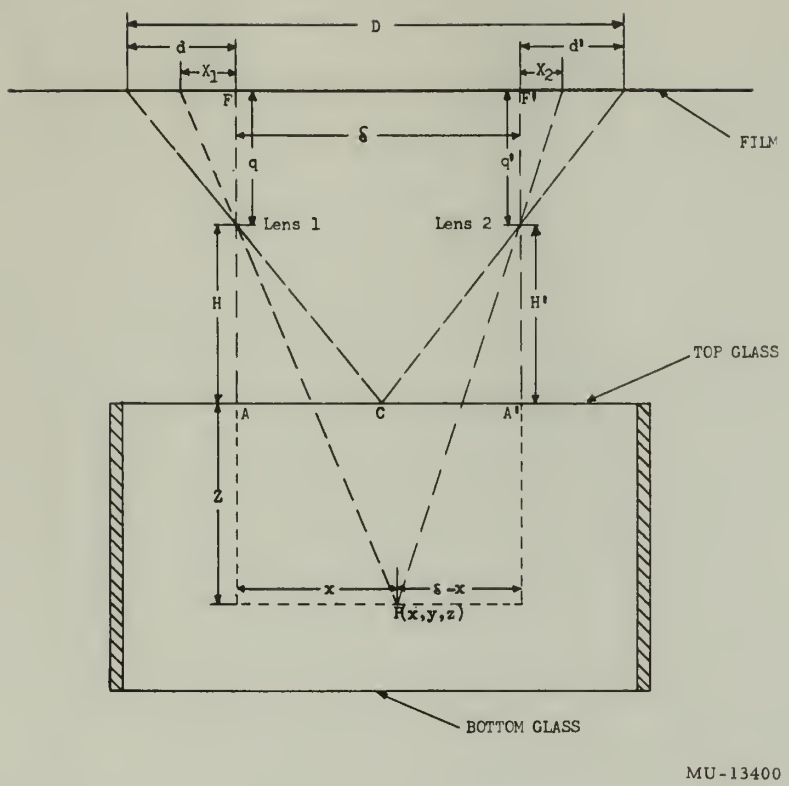

Fig. 11. Line drawing of 10-inch bubble chamber optical system

available from direct measurement; we must determine x, y, and z. Using Fig. 11, then, we have

$$x/(H + z) = - X_1^I/q$$

and

$$(\delta - x)/(H + z) = X_1^{II}/q;$$

solving these for H + z, we obtain

$$H + z = - x\,(q/X_1^I) = (\delta - x)\,(q/+ X_1^{II}), \qquad (A.3)$$

$$x = (\,[H + z]/q)\, X_1^I = k_1 X_1^I;\ k_1 = \delta/(X_1^I - X_1^{II}), \qquad (A.4)$$

where k_1 is the magnification in the z plane containing the point P. Similarily it can be shown that we have

$$y = k_1 Y_1^I .$$

Substituting Eq. (A.4) into (A.3), we get

$$z = k_1 q - H.$$

Finally, for the range of the μ^+, we have

$$r = (\overline{\Delta x}^2 + \overline{\Delta y}^2 + \overline{\Delta z}^2)^{1/2} ,$$

where

$$\Delta x = k_1 X_1^I - k_2 X_2^I ,$$

$$\Delta y = k_1 Y_1^I - k_2 Y_2^I ,$$

$$\Delta z = q(k_1 - k_2) .$$

BIBLIOGRAPHY

1. D. Glaser, Phys. Rev. 87, 665 (1952).
2. H. C. Dittler and T. F. Gerecke, Liquid Hydrogen Bubble Chambers (M.S. Thesis), UCRL-2985, May 1955.
3. H. A. Bethe, Ann. Physik 5, 325 (1930).
4. F. Bloch, Ann. Physik 16, 285 (1933).
5. W. R. Fry, Phys. Rev. 86, 418L (1952); S. Lokanathan and J. Steinberger, Bull. Am. Phys. Soc. 29, No. 7, Q12 (1954).
6. K. M. Crowe, Nuovo cimento 3, 541 (1957).
7. W. A. Aron, The Passage of Charged Particles Through Matter (Thesis), UCRL-1325, May 1951.
8. E. J. Williams, Proc. Cambridge Phil. Soc. 33, 179 (1937).
9. Cohen, Crowe, and DuMond, The Fundamental Constants of Physics (Interscience, New York, to be published).
10. Blumberg, Gow, and Schwemin, Proc. 1956 Cryogenic Engs. Conf., Boulder, Colo., Paper H-1.
11. White, Friedman, and Johnston, J. Am. Chem. Soc. 72, 3927 (1950).
12. W. I. Linlor and Q. A. Kerns, Bubble Chamber Pressure Gage, UCRL-3173, Oct. 1955.
13. M. Lynn Stevenson, UCRL ENG. Note 4310-03, M-13A (1956) (unpublished).
14. Johnston, Keller, and Friedman, J. Am. Soc. 76, 1482 (1954).
15. A. Eucken, Verhandl. deut. physik. Ges. 18, 4 (1916).
16. H. Gutsche, Z. physik. Chem. (A), 184, 45 (1939).
17. Woolley, Scott, and Brickwedde, NBS J. Research 41, 379 (1948).
18. G. G. Bower, Control Engineering 4, 107 (1957).
19. E. Segrè and R. Mather, Phys. Rev. 84, 191 (1951).
20. Mathias, Crommelin, and Kammerlingh Onnes, Leiden Univ. Phys. Lab. Comm. 14, 154b (1921).
21. N. Bohr, Penetration of Atomic Particles Through Matter, I Kommission Hos Ejnar (Munksgaard, København, 1948).

Thesis 35701
C4817 Clark
Range-energy relation for liquid hydrogen bubble chambers.